Title
ANGULAR-MOMENTUM EFFECTS ON NEUTRON EMISSION BY Dy and Tb COMPOUND NUCLEI

Authors
Simonoff, Gabriel N.
Alexander, John M.

Publication Date
1962-09-01

University of California

Ernest O. Lawrence Radiation Laboratory

ANGULAR-MOMENTUM EFFECTS ON NEUTRON EMISSION BY Dy AND Tb COMPOUND NUCLEI

Berkeley, California

DISCLAIMER

Submitted to Journal Physical Review

UCRL-10099-Rev.

UNIVERSITY OF CALIFORNIA

Lawrence Radiation Laboratory
Berkeley, California

Contract No. W-7405-eng-48

ANGULAR-MOMENTUM EFFECTS ON NEUTRON EMISSION BY Dy AND Tb COMPOUND NUCLEI

Gabriel N. Simonoff and John M. Alexander

September, 1962

ANGULAR-MOMENTUM EFFECTS ON NEUTRON EMISSION BY Dy AND Tb COMPOUND NUCLEI

Gabriel N. Simonoff and John M. Alexander

Lawrence Radiation Laboratory
University of California
Berkeley, California

September, 1962

ABSTRACT

We have studied as a function of energy three reactions producing 4.1-h Tb^{149g} from Tb compound nuclei and nine reactions producing Dy products from Dy compound nuclei. Incident particles were B^{10}, B^{11}, C^{12}, and O^{16} of energy 4 to 10.4 MeV per amu. Measurements of the average recoil range give strong evidence that all these reactions proceed by compound-nucleus formation. We report angular distributions of the final heavy products for all these reactions. From angular distribution data we deduce the average total energies of photons and neutrons for each reaction. In the Tb reactions the average total photon energy is always less than 12 MeV. In the Dy reactions the average total photon energy varies linearly with total available energy from nearly 0 to about 30 MeV. These large differences in total photon energy are attributed to differences in the angular momenta of the initial compound nuclei. The rate of increase of the average kinetic energy of all neutrons (from Dy systems) is approximately proportional to the square root of the excitation energy. For a given excitation energy of the Dy systems the average total photon energy does not appear to vary with average angular momentum.

ANGULAR-MOMENTUM EFFECTS ON NEUTRON EMISSION BY Dy AND Tb COMPOUND NUCLEI*

Gabriel N. Simonoff†‡ and John M. Alexander

Lawrence Radiation Laboratory
University of California
Berkeley, California

I. INTRODUCTION

In this paper, we attempt to gain information on the average energies of neutrons and photons emitted from compound nuclei excited to energies up to approx 125 MeV. We attempt to separate effects of angular momentum (J) from effects of excitation energy (Ex) by the comparison of compound nuclei having similar values of Z, A, and Ex but differing values of J. The products Dy^{149}, Dy^{150}, and Dy^{151} were observed from the compound systems $_{66}Dy^{154}$ (formed by C^{12} + Nd^{142}), and Dy^{156} (formed by two reactions, C^{12} + Nd^{144} and O^{16} + Ce^{140}). Also, the product Tb^{149g} has been observed from several Tb compound nuclei. Cross-section data imply that the latter reactions proceed from compound systems with $J \lesssim 7.5\ \hbar$[1], whereas the former reactions involve much higher average angular momenta.[2]

In this work and in previous studies average range measurements have been used to test the reaction mechanism.[3] These measurements give strong evidence that the reactions we study are reactions in which the neutrons are emitted with angular distributions symmetric about 90 deg.

We report angular distribution measurements for the products previously mentioned. A relationship between total neutron energy and root-mean-square angle has been derived. This relationship assumes isotropic neutron emission but is not extremely sensitive to this assumption. Using this relationship and our angular distribution measurements, we obtain average total neutron

energies and total photon energies associated with each individual reaction. In a subsequent paper[4] that presents cross section data we discuss the overall energy and angular momentum balance for these reactions.

We conclude that the low-spin Tb compound nuclei that decay to Tb^{149g} dissipate less than about 12 MeV in photons. The amount of photon emission from Dy compound nuclei of higher spin is quite different. This qualitative result was previously obtained by Morton, Choppin and Harvey.[5] Mollenauer has reported observations of photons emitted in complex nuclear reactions.[6] His results also indicate that total photon energies increase with increasing J of the compound nucleus. Our results imply that total photon energies up to about 30 MeV are associated with neutron emission from Dy compound nuclei. The average kinetic energy of the emitted neutrons is approximately proportional to $\sqrt{Ex.}$ The average total photon energy increases with increasing Ex or J, or both, but is not proportional to $\langle J^2 \rangle$.

II. RECOIL EFFECTS OF THE COMPOUND-NUCLEUS MECHANISM

The basic features of the compound-nucleus mechanism are the following. A projectile and a target nucleus interact to form an excited compound system having a mean life that is long compared with the time required for the projectile to traverse the nuclear diameter. The excited compound nucleus decays by emitting particles and photons until a stable or radioactive final product is formed. The angular distribution of the emitted particles or photons is symmetric about $\pi/2$ in the frame of reference of the compound nucleus if the level density of the residual nucleus is large enough to justify the random-phase approximation.[7] In this work we study systems with initial excitation energies of about 50 to 125 MeV, and thus we assume that this approximation is justified.

Let us consider in detail the consequences of this mechanism for two recoil properties of the final products: (a) range-straggling parameter ρ, and (b) root-mean-square angle (laboratory system), $\langle\theta_L^2\rangle^{1/2}$. Let $\underset{\sim}{v}$ denote the velocity given the compound nucleus by the initial impact of the projectile (this is identical to the velocity of the center of mass). Let $\underset{\sim}{V}$ denote the velocity in the c.m. system given to the final product by the evaporation of particles. Let θ denote the c.m. angle between $\underset{\sim}{v}$ and $\underset{\sim}{V}$ and let θ_L denote the lab angle between $\underset{\sim}{v}$ and $\underset{\sim}{v} + \underset{\sim}{V}$. The angular distribution of $\underset{\sim}{V}$ is designated by $W(\theta)$, and the recoil distance is taken as equal to $k\,|\underset{\sim}{v} + \underset{\sim}{V}|^N$, where k and N are constants. The projection R of the recoil distance on the beam direction is given by

$$R = k\,|\underset{\sim}{v} + \underset{\sim}{V}|^N \cos\theta_L .$$

If we have the average quantity $\langle V^2 \rangle << v^2$, and if $W(\theta)$ is symmetric about $\pi/2$, then the average projection of the ranges on the beam direction, R_0, can be considered to depend only on v, k, and N — and to be independent of V and $W(\theta)$.[8] The average range R_0 of the product should be associated with a recoil energy E_R such that

$$E_R = \frac{E_b A_b A_R}{(A_b + A_T)^2} \qquad (1)$$

where mass number is denoted by A, with subscript b indicating the bombarding particle subscript R the recoil atom or final product and subscript T the target. The kinetic energy of the projectile in the laboratory system is denoted by E_b.

The contribution to the measured range straggling from the distribution of $\underset{\sim}{v} + \underset{\sim}{V}$ is given by

$$\langle (R-R_0)^2 \rangle = \frac{1}{2} \int_0^{\pi} [R(v,V,\theta) - R_0(v,V)]^2 \, W(\theta) \sin\theta \, d\theta. \qquad (2)$$

This integral has been evaluated by substituting the appropriate functions of velocity for R and R_0. For $V << v$, and for $W(\theta) = 1$ we have, to order $(V/v)^3$,

$$\frac{\langle (R-R_0)^2 \rangle}{R_0^2} = \frac{N^2 \langle V^2 \rangle}{3v^2} \; ; \qquad (3)$$

for $W(\theta) = a + b \cos^2\theta$,

$$\frac{\langle (R-R_0)^2 \rangle}{R_0^2} = \frac{N^2 \langle v^2 \rangle [1 + (3b/5a)]}{3v^2 [1 + (b/3a)]} ; \tag{4}$$

and for $W(\theta)$ proportional to $1/\sin\theta$,

$$\frac{\langle (R-R_0)^2 \rangle}{R_0^2} = \frac{N^2 \langle v^2 \rangle}{2v^2} . \tag{5}$$

Detailed calculations by the Monte Carlo method have shown that for $V^2 << v^2$ the range distribution due to evaporation effects can be closely approximated by a Gaussian distribution with straggling parameter denoted by ρ_n.[9] Thus we have

$$\rho_n^2 = \frac{\langle (R-R_0)^2 \rangle}{R_0^2} . \tag{6}$$

The average square of the angle $\langle \theta_L^2 \rangle$ of the recoil atoms is given by

$$\langle \theta_L^2 \rangle = \frac{1}{2} \int_0^{\pi} \left\{ \tan^{-1} \frac{V \sin\theta}{v + V\cos\theta} \right\}^2 W(\theta) \sin\theta \, d\theta . \tag{7}$$

To order $(V/v)^3$ for $W(\theta) = 1$ we have

$$\langle \theta_L^2 \rangle = \frac{2 \langle v^2 \rangle}{3v^2} . \tag{8}$$

For $W(\theta) = a + b \cos^2 \theta$ we have

$$\langle \theta_L^2 \rangle = \frac{2\langle V^2 \rangle [1 + (b/5a)]}{3v^2[1 + (b/3a)]} . \qquad (9)$$

For $W(\theta)$ proportional to $1/\sin \theta$ we have

$$\langle \theta_L^2 \rangle = \frac{\langle V^2 \rangle}{2v^2} . \qquad (10)$$

The equations given above show relationships between some observable properties and the magnitude of the velocities $\underset{\sim}{v}$ and $\underset{\sim}{V}$. The velocity $\underset{\sim}{v}$ is, of course, specified by the momentum of the projectile and the mass of the compound nucleus:

$$v^2 = \frac{2A_b E_b}{(A_b + A_T)^2} . \qquad (11)$$

The value of $\langle V^2 \rangle$ is determined by the average total kinetic energy T_n of the emitted particles in the c.m. system and by their angular and energy distributions. The recoil velocity due to emission of photons can be neglected.

Assume that the compound nucleus emits nucleons in random directions then $W(\theta) = 1$, and we have $\langle P^2 \rangle = 2 T_n$, where P is the resultant momentum of the final product. Then we can approximate the recoiling mass by $\frac{1}{2} (A_b + A_T + A_R)$, and we have

$$\langle V^2 \rangle = \frac{8T_n}{(A_T + A_b + A_R)^2} . \qquad (12)$$

The total energy available in the c.m. system is $E_{c.m.} + Q$, therefore the average total energy emitted as photons T_γ is

$$T_\gamma = E_{c.m.} + Q - T_n \quad . \tag{13}$$

Thus, from Eqs. (3),(6),(11) and (12) we have

$$\rho_n^2 = \frac{4N^2 T_n (A_b + A_T)^2}{3E_b A_b (A_b + A_T + A_R)^2} \quad , \tag{14}$$

and from Eqs. (8),(11) and (12) we have

$$\langle \theta_L^2 \rangle = \frac{(8T_n)(A_b + A_T)^2}{(3E_b A_b)(A_b + A_T + A_R)^2} \quad . \tag{15}$$

In all these relationships the neutron mass is taken as unity.

If the angular distribution of the emitted particles is not isotropic, the development is much more complicated. However, from Eqs. (5) and (10) one can see that even an extreme case of $W(\theta) \propto 1/\sin\theta$ leads to changes of only about 25% in ρ_n, and about 15% in $\langle \theta_L^2 \rangle^{1/2}$.

III. EXPERIMENTAL TECHNIQUES AND RESULTS

In our experiments we have made observations of the nuclides 4.1-h Tb^{149g}, 7.4-min Dy^{150}, and 17.9-min Dy^{151}. These are the only known alpha-emitting nuclides in the rare-earth region that have convenient decay periods and favorable alpha branching ratios. Therefore, measurement of the alpha radioactivity by ionization chambers allows us to identify these specific products without chemical analysis, thus eliminating chemical-yield errors.

In other work we have observed that cross sections for Tb^{149g} from Tb compound nuclei are very small.[1] Also Dy^{150} and Dy^{151} cross sections from Dy compound nuclei are very large.[4] The excitation functions for Dy^{149} + Tb^{149g} from Dy compound nuclei closely resemble those for Dy^{150} and Dy^{151}.[4] We infer that a dominant fraction of the Tb^{149g} that is observed from Dy compound nuclei actually comes from radioactive decay of Dy^{149} to Tb^{149g}. Therefore we refer to the recoil properties of Tb^{149g} produced from Dy compound systems as those of Dy^{149}.

A. Range Measurements

The range measurements were made with thin targets (30 to 100 $\mu g/cm^2$), and thin Al catcher foils (approx 150 $\mu g/cm^2$), as described previously.[3,8] On a probability scale, F_t, the fraction of the total activity that passed through catcher foils of combined thickness t, was plotted against t. These probability plots always indicate that the range distribution can be described as a Gaussian function with two parameters (the average range R_0 and the straggling parameter ρ):

$$P(R)dR = \frac{1}{R_0\rho(2\pi)^{1/2}} \exp\left[-\left(\frac{R-R_0}{\sqrt{2}\,R_0\rho}\right)^2\right] dR. \qquad (16)$$

The results of the range measurements are given in Table I. The first three columns give the reaction, beam energy, and observed product, respectively. The values of the measured quantities R_0 and ρ are given in the fourth and fifth columns. The measured straggling parameter is the result of contributions from several sources: (a) finite target thickness ρ_W, (b) catcher-foil inhomogeneities ρ_f, (c) inherent straggling in the stopping process ρ_s, and (d) the nuclear reaction ρ_n. If all these contributions are treated as Gaussian we have

$$\rho_n^2 = \rho^2 - \rho_W^2 - \rho_f^2 - \rho_s^2 . \qquad (17)$$

The effects of ρ_W, ρ_f, and ρ_s have been subtracted as previously described,[3] and we show the values of ρ_n in the last column.

The values of ρ_n are not accurate enough to use in a quantitative way. We can only say that the values of ρ_n are not inconsistent with any conclusions deduced from the angular-distribution results. As shown in Eqs. (14) and (15), the values of ρ_n and $\langle\theta_L^2\rangle^{1/2}$ are both related to T_n. The major result from the range measurements is the determination of the average range R_0.

B. Angular-Distribution Measurements

The angular-distribution measurements were performed by essentially the same method as developed by Harvey et al.[5,10] A thin target layer was exposed to a collimated beam from the Berkeley Hilac. The Nd^{144}, Nd^{146}, and Ce^{140} targets were prepared from enriched isotopes obtained from the Oak Ridge National Laboratory. The enrichments were 97.4% Nd^{142}, 97.3% Nd^{144}, 96.2% Nd^{146}, and 99.6% Ce^{140}. A thick (0.001-in.) Al catcher foil was placed at some distance from the target; and the catcher was cut into rings concentric about the beam.

The geometry of the appartus is shown in Fig. 1. The angular resolution of the beam was defined by two 1/16-in. collimators to approx 0.5 deg in some experiments. In others the second collimator was 1/8 in. in diameter, giving rise to an angular definition of approx 1 deg. The effect of the size of the second collimator was measured experimentally (see Table IV).

The catcher foil was cut by a stainless steel cutter and a hydraulic press into rings of 1/8-in. radial dimension. Each ring subtended approx 1 deg. Two different cutters were used. The dimensions of these cutters were carefully calibrated by weighing several sets of rings cut from sheets of uniform Al foil. The angles defined by each ring are given in Table II.

The results of all angular-distribution measurements are given in Table III. The first two columns give the beam energy and target thickness, respectively. As shown in Table II, the two cutters had slightly different dimensions. Therefore, for each experiment we give the cutter, and, for each ring, the fractional cross section per unit angle

$\Delta\sigma/\sigma\Delta\theta$. The average angle $\langle\theta_L\rangle$ was calculated by the relationship

$$\langle\theta_L\rangle = \sum_i (\Delta\sigma_i/\sigma)\langle\theta_i\rangle \qquad (18)$$

where $\langle\theta_i\rangle$ is the mean angle of the ith ring and $\Delta\sigma_i/\sigma$ is the fraction of the total activity observed in that ring. The root-mean-square angle was similarly calculated:

$$\langle\theta_L^2\rangle^{1/2} = \left[\sum_i (\Delta\sigma_i/\sigma)\,\langle\theta_i^2\rangle\right]^{1/2} , \qquad (19)$$

where $\langle\theta_i^2\rangle$ is the mean squared angle of the ith ring. Values of $\Delta\sigma_i$ less than 2% of the maximum value of $\Delta\sigma_i$ were not included in the summations.

The effect of target thickness on the angular distribution of Tb^{149} was carefully studied for several cases. One series of these experiments is shown in Fig. 2. The values of $\langle\theta_L\rangle$ and $\langle\theta_L^2\rangle^{1/2}$ change significantly but not very rapidly with the target thickness, as shown in Fig. 3. We have used the values of $d\langle\theta_L\rangle/dW$ and $d\langle\theta_L^2\rangle^{1/2}/dW$ shown in Fig. 3 to correct these average properties to zero target thickness. The assumption was made that all reactions of the same projectile have the same value of $d\langle\theta_L\rangle/dW$ and $d\langle\theta_L^2\rangle^{1/2}/dW$. This is probably a very good approximation (especially for the C^{12} and O^{16} experiments), because the angular distributions and recoil velocities are very similar. The detailed angular distributions in Table III for $W = 0$ were obtained by linearly extrapolating $\Delta\sigma/\sigma\Delta\theta$ to $W = 0$ for each ring. This procedure becomes more uncertain, of course, with increasing angle.

The effect of collimator size was carefully studied for two different cases (Nd^{144} + 122.8-MeV and 77.5-MeV C^{12}). The angular distribution was

measured with two 1/16-in. collimators (angular definition $\approx$ 0.5 deg.) and in a separate experiment with the second collimator 1/8 in. (angular definition $\approx$ 1 deg.). The average angles $\langle\theta_L\rangle$ and $\langle\theta_L^2\rangle^{1/2}$ were enlarged by 0.25 and 0.30 deg respectively by the poorer angular definition of the beam. We assume that no correction is necessary for experiments with two 1/16-in. collimators, and for the other experiments we correct the average angles by the above values. The corrected values of the average angles are given in Table IV along with average energies that are discussed later.

IV. DISCUSSION

A. Ranges

In preceding papers we have presented an internal-consistency argument for using average range values to test the validity of the compound-nucleus model.[3] The lack of independent range-energy data for heavy recoil atoms necessitates this kind of treatment. First, assume that the compound-nucleus mechanism is valid. Thus Eq. (1) should give the recoil energy E_R, appropriate to the average range R_0. Then the values of R_0 are plotted versus E_R, as in Fig. 4. From this figure we see that one smooth curve fits all the measurements. Furthermore, this curve is the same as is consistent with Tb^{149} range measurements from many other reactions.[3] This test implies that Eq. (1) gives a correct description of the recoil energy or, in other words, that the projectile transfers all its momentum to the compound system. We conclude that the most likely mechanism for all these reactions is compound-nucleus formation, followed by emission of particles with forward-backward symmetry. All further discussion is based on this conclusion.

B. Angular Distributions

From the average recoil-range measurements we have concluded that all the reactions studied here proceed by reactions for which the angular distribution of the emitted neutrons is essentially symmetric about $\pi/2$ in the center-of-mass system. We use measurements of the angular distribution of the final products to calculate average kinetic energy of the neutrons and also average total photon energies.

The angular distribution of the final products depends on the energy and angular distributions of the emitted neutrons (see Sec. II). If the

neutrons are emitted only as s waves, then their emission is isotropic. However, if neutrons are emitted with nonzero ℓ values, then forward-backward peaking is expected.[7] The classical limit to this forward-backward preference is given by an angular distribution of the form[7]

$$W(\theta) \propto 1/\sin \theta .$$

Experimental studies of heavy-ion reactions have shown that alpha particles and fission fragments are emitted with angular distributions approaching this limit; neutrons and protons are emitted with much less forward-backward peaking.[11] Ericson's formulation of this problem leads us to expect that most of the neutrons are emitted with nearly isotropic angular distributions.[7] As shown in Section II, the value of $\langle\theta_L^2\rangle^{1/2}$ is not very sensitive to small anisotropies in neutron emission.

Let us assume initially that all neutrons are emitted isotropically. From Eqs. (13) and (15) we can calculate the average energy emitted as photons, and the average kinetic energy of the neutrons for each reaction. The results of these calculations are given in Table IV. First we give the bombarding energy; then the average angles $\langle\theta_L\rangle$ and $\langle\theta_L{}^2\rangle^{1/2}$ corrected for target thickness and angular definition of the beam. In the last three columns we give the total available energy (Seeger's mass formula was used[12]), the average total kinetic energy of the neutrons, and average total photon energy. We estimate that the values of T_n have a standard error from experimental sources of not more than about 10%.

If the neutrons are not emitted isotropically, the true energies will differ from those given in Table IV. The maximum alteration due to this effect can be estimated from Eq. (10), which indicates that $\langle\theta_L{}^2\rangle$ for isotropic neutron emission is approx 33% greater than for $W(\theta) \propto 1/\sin\theta$.

Thus, if all the neutrons are emitted with this extremely anisotropic angular distribution, then the neutron kinetic energies should be increased by about 33% (see Eq. 15). Also, the total photon energies should be correspondingly decreased (see Eq. 13). In this paper we proceed with the discussion based on the approximation of isotropy. For this reason the neutron energies in Table IV are probably somewhat too small, and the photon energies are too large. Note that these errors are systematic. Therefore they probably have only a small effect on the dependence of T_n and T_γ on reaction type and bombarding energy. Precise measurements of range straggling due to the velocity distribution would give a test of this approximation.

In Fig. 5 we plot the average total photon energy T_γ against the total available energy. There is a striking difference between the reactions leading to Dy^{149}, Dy^{150}, Dy^{151} and those leading to Tb^{149g}. Increasing the available energy leads to a rather slowly increasing photon energy for Tb^{149g} reactions. But for Dy reactions most of the available energy greater than about 10 or 15 MeV is dissipated by photon emission.

There is a small internal inconsistency in the T_γ values that we have calculated. These values become negative for two cases; this effect is on the border line of our experimental errors. Also this result depends on the masses used to calculated Q values. We have used Seeger's mass formula for both the target and heavy product nuclei.[12] If the angular distribution of the neutrons is peaked forward and backward, this inconsistency is even more pronounced.

As discussed in another paper, the reactions leading to Tb^{149g} probably involve only systems of low angular momentum ($\lesssim 7.5\ \hbar$).[1] The results of this study imply that for these Tb compound nuclei of low spin

photon emission does not compete favorably with neutron emission. The reactions leading to Dy^{149}, Dy^{150}, and Dy^{151} have very high cross sections;[4] thus the observed products must be formed from compound nuclei that have angular momentum distributions typical of most compound systems.[2] Presumably, this primary angular-momentum distribution gives rise to a large number of compound nuclei of high spin.[2] As the excited nuclei decay, the angular momentum must be removed by particle and photon emission. Angular momentum barriers increase the lifetime for neutron emission, and thus photon emission becomes a competitive process. Grover has described the features of this competition.[13]

Another way of presenting our experimental results is to plot the average energies per emitted neutron versus the available energy per neutron $(E_{c.m.} + Q)/x$. These plots are shown in Fig. 6. Plots of cross section versus available energy per neutron lead to very similar results for these and other similar reactions. The reactions (HI, xn) Dy^{149}, Dy^{150}, Dy^{151} all peak at about 5.9 MeV per neutron.[4] The reactions (HI, xn) Tb^{149g} all peak at 3 to 4 MeV per neutron.[1]

The Tb^{149g} reactions give values of T_n and T_γ that are expected from evaporation theory without angular momentum effects. Increasing available energy goes mainly into kinetic energy of the neutrons. For Dy reactions the average kinetic energy of the neutrons increases rather slowly with available energy. For the smaller available energies almost no energy goes to photons. For the higher available energies the photon and neutron energies are comparable.

It has frequently been assumed that the classical rotational energy of a compound nucleus is not available for nuclear evaporation.[14] Thus this

rotational energy is expected to be disipated by additional photon emission. Our results, however, are not consistent with this idea. The reactions of C^{12} with Nd^{144} and of O^{16} with Ce^{140} both form Dy^{156} compound nuclei. Over the energy region of our studies, the average squared angular momenta differ by about 25% for a given value of the excitation energy. And yet, in Figs. 5 and 6 the values of T_n and T_γ are usually indistinguishable. A possible exception is for Dy^{149} productions at energies near threshold.

These values of average neutron and photon energies are associated with specific reactionsinvolving neutron emission. Mollenauer's observations of photons are, on the other hand, not associated with such specific reactions. By reference to the excitation functions, we can extract information about average energies of all neutron-emitting reactions. Excitation functions for all the (HI, xn) Dy^{149}, Dy^{150}, Dy^{151} reactions peak at about 5.9 MeV per emitted neutron.[4] Thus, if we compare T_n and T_γ values at 5.9 MeV per neutron, we get a measure of the variation of these quantities with number (x) of neutrons or excitation energy (Ex). The values of the average neutron energies (at 5.9 MeV per neutron) in Fig. 6 are proportional to $(Ex)^{0.4\pm0.15}$. The average photon energy per emitted neutron correspondingly decreases with Ex. The excitation functions give information related to the energy and angular momentum of the first neutron emitted in the evaporation cascade. A more detailed comparison of the results of this study with excitation function measurements is given in a following paper.[4]

C. Conclusions

To summarize this study we may list the following conclusions: (a) The reactions involving neutron emission that we have studied proceed by compound-nucleus formation. (b) The decay of Dy^{156} excited to 65 to 125 MeV is almost the same for $C^{12} + Nd^{144}$ and for $O^{16} + Ce^{140}$ in spite of a difference of about 25% in $\langle J^2 \rangle$. Compound nuclei of low spin (as measured by reactions forming Tb^{149g}) have very different decay properties from those of high spin (as measured by reactions forming Dy^{149}, Dy^{150}, and Dy^{151}). (d) The low-spin compound systems dissipate less than about 12 MeV in photons; the remaining energy appears as kinetic energy of the emitted neutrons. (e) The compound systems of higher spin dissipate, on the average, about one-half their available excitation energy by photon emission. (f) For a given reaction, the average total photon energy (T_γ) increases almost linearly with the available energy, and extends to T_γ values of approximately 30 MeV for available energies of 50 to 60 MeV. (g) The average kinetic energy of the neutrons increases approximately as the square root of the excitation energy.

ACKNOWLEDGMENTS

Dan O'Connell and Gordon Steers did a fine job of preparing targets. The Hilac crew worked hard to get a beam through two 1/16 in. collimators. We thank L. Altman, J. R. Grover and E. K. Hyde for initial reading of the manuscript.

FOOTNOTES AND REFERENCES

*Work done under the auspices of the U. S. Atomic Energy Commission.

†On leave from Laboratorie Joliot Curie de Physique Nucléaire Orsay, France.

‡Present address: Nouvelle Faculté des Sciences de Bordeaux, Talence (Gironde) France.

1. J. M. Alexander and G. N. Simonoff, Excitation Functions for Tb^{149g} from Reactions Between Compled Nuclei (UCRL-10525, Oct. 1962) (to be submitted to Phys. Rev.).
2. T. D. Thomas, Phys. Rev. 116, 703 (1959).
3. J. M. Alexander and L. Winsberg, Phys. Rev. 121, 529 (1961); J. M. Alexander and D. H. Sisson, Phys. Rev., Dec. 1962 (in press).
4. J. M. Alexander and G. N. Simonoff, UCRL-10541, 1962 (unpublished).
5. J. R. Morton III, G. R. Choppin, and B. G. Harvey, Phys. Rev. 128, 265 (1962).
6. J. F. Mollenauer, Phys. Rev. 127, 867 (1962).
7. D. C. Peaslee, Ann. Rev. Nuclear Sci. 5, 99 (1955); T. Ericson, Advances in Physics, edited by N. F. Mott (Taylor and Francis, Ltd., London, 1960), Vol. 9, p. 425.
8. L. Winsberg and J. M. Alexander, Phys. Rev. 121, 518 (1961).
9. J. M. Alexander, L. Altman, and S. Howry (Lawrence Radiation Laboratory), unpublished calculations.
10. P. F. Donovan, B. G. Harvey, and and W. H. Wade, Phys. Rev. 119, 218 and 225 (1960).
11. W. J. Knox, A. R. Quinton and C. E. Anderson, Phys. Rev. 126, 2120 (1960); H. C. Britt and A. R. Quinton, Phys. Rev. 120, 1768 (1960); V. E. Viola, Jr., T. D. Thomas, and G. T. Seaborg, (UCRL-10248, 1962), to be submitted to Phys. Rev. H. W. Broek, Phys. Rev. 124, 233 (1961).

12. P. A. Seeger, Nuclear Phys. 25, (1961).

13. J. R. Grover, Phys. Rev. 127, 2142 (1962); 128, 267 (1962).

14. G. A. Pik-Pichak, Soviet Physics JETP. 11, 557 (1960).

Table I. Range measurements in Al.

Reaction	Bombarding energy, E_b (lab) (MeV)	Observed product	Average range, R_o (mg/cm^2)	Measured straggling parameter, ρ	Nuclear reaction straggling parameter, ρ_n [a]
$Ce^{140} + O^{16}$	146.0	Tb^{149}	0.996	0.183	0.09±0.035
		Dy^{150}	0.991	0.190	0.102±0.03
	140.0	Tb^{149}	0.953	0.186	0.083±0.04
		Dy^{150}	0.958	0.197	0.105±0.03
	128.1	Tb^{149}	0.910	0.196	0.089±0.033
		Dy^{150}	0.912	0.202	0.10±0.03
	112.4	Tb^{149}	0.803	0.193	≈ 0
	100.4	Dy^{151}	0.758	0.200	≈ 0
	100.0	Dy^{151}	0.730	0.196	≈ 0
	88.2	Dy^{151}	0.677	0.199	≈ 0
$Nd^{144} + C^{12}$	120.5	Tb^{149}	0.661	0.245	0.082±0.03
		Dy^{150}	0.656	0.248	0.085±0.03
	95.0	Tb^{149}	0.549	0.224	≈ 0
		Dy^{150}	0.551	0.223	≈ 0
		Dy^{151}	0.554	0.237	≈ 0

[a] The value of ρ_n is given only if it is significantly different from zero.

Table II. Angles defined by each cutting edge (deg).[a]

Ring number	Cutter 1	Cutter 2
	0	0
1	1.16	1.04
2	2.10	2.04
3	3.12	3.07
4	4.15	4.12
5	5.16	5.15
6	6.16	6.18
7	7.15	7.17
8	8.17	8.21
9	9.19	9.19
10	10.19	10.19
11	11.18	11.16
12	12.13	12.15
13	13.14	13.17
14	14.15	14.10
15	15.08	15.08
16	16.02	16.06

[a] For each ring the inner and outer angles are given. The outer angle for any ring is the inner angle for the next

Table III. Angular distribution results (Continued)

Bombarding energy, E_b (lab) (MeV)	Target thickness W ($\mu g/cm^2$)	Cutter	Fractional cross section per unit angle $\Delta\sigma/\sigma\Delta\theta$ (deg^{-1}) — Ring number 1	2	3	4	5	6	7	8	9	10	11	12	13	14	15	16	17	18	$\langle\theta_L\rangle$	$\langle\theta_L^2\rangle^{1/2}$
			$Nd^{144}(C^{12}, 5n)Dy^{151}$																				
77.5	77.0	2	0.036	0.086	0.123	0.140	0.137	0.115	0.096	0.074	0.052	0.038	0.025	0.018	0.015	0.011	(0.007)	(0.005)	(0.004)		5.39	6.26
77.5	77.0	1[b]	0.039	0.080	0.116	0.139	0.127	0.119	0.101	0.076	0.054	0.041	0.027	0.021	0.015	0.014	(0.008)	(0.006)	(0.004)	(0.003)	5.63	6.56
83.4	30.9	2	0.040	0.100	0.135	0.149	0.140	0.117	0.105	0.075	0.047	0.029	0.014	0.013	0.010	(0.005)	(0.003)				4.94	5.66
94.0	30.9	1	0.050	0.089	0.114	0.129	0.133	0.137	0.101	0.080	0.059	0.037	0.024	0.013	0.010	(0.006)	(0.004)	(0.003)			5.25	5.88
			$Nd^{144}(C^{12}, 6n)Dy^{150}$																				
94.0	30.9	1	0.048	0.088	0.114	0.146	0.149	0.117	0.099	0.072	0.048	0.037	0.027	(0.017)	(0.012)	(0.008)	(0.006)	(0.004)			5.24	6.04
99.7	30.9	2	← 0.054 →		← 0.129 →		0.147	0.131	0.107	0.082	0.061	0.038	← 0.014 →		0.012	0.006	(0.003)				5.22	5.93
111.6	30.9	1	← 0.049 →		← 0.120 →		0.133	0.133	0.109	0.086	0.066	0.045	← 0.024 →		0.012	0.008	0.005	(0.003)			5.56	6.33
122.8	76.8	1	← 0.044 →		← 0.096 →		0.115	0.126	0.106	0.092	0.078	0.058	← 0.037 →		0.029	0.016	0.012	0.005			6.24	7.09
			$Nd^{144}(C^{12}, 7n)Dy^{149}$																				
94.0	30.9	1	(0.054)	0.085	0.119	0.152	0.146	0.120	0.106	0.077	0.046	0.028	0.018	0.014	0.011	(0.006)	(0.004)				5.03	5.76
99.7	30.9	2	← 0.067 →		0.121	0.139	0.143	0.129	0.103	0.075	0.051	0.035	← 0.016 →		0.008	0.006	(0.003)				5.05	5.80
111.6	30.9	1	0.034	0.082	0.118	0.139	0.138	0.126	0.103	0.088	0.057	0.039	← 0.020 →		0.012	(0.008)	(0.005)	(0.004)			5.40	6.15
122.8	30.9	2[b]	← 0.047 →		← 0.112 →		0.130	0.129	0.110	0.090	0.068	0.048	0.035	0.024	0.013	0.008	0.006	(0.004)			5.73	6.51
122.8	10.8	1	← 0.058 →		← 0.125 →		0.141	0.126	0.110	0.084	0.063	0.040	← 0.022 →		0.008	0.004	0.002				5.21	6.01
122.8	30.9	2	← 0.051 →		← 0.121 →		0.135	0.126	0.111	0.086	0.065	0.046	← 0.022 →		0.012	0.007	0.004				5.48	6.22
122.8	76.8	1	← 0.046 →		← 0.111 →		0.120	0.122	0.105	0.091	0.069	0.053	← 0.032 →		0.018	0.012	0.009	0.006	(0.004)	(0.003)	6.01	6.88
122.8	0		← 0.057 →		← 0.127 →		0.145	0.128	0.110	0.083	0.062	0.039	← 0.018 →		0.007	0.003	0.0015				5.09	5.84
			$Ce^{140}(O^{16}, 5n)Dy^{151}$																				
89.7	36.4	2	0.062	0.142	0.187	0.188	0.167	0.100	0.063	0.030	0.014	0.010	0.006	0.006							3.85	4.40
101.0	36.4	1	0.053	0.142	0.186	0.189	0.145	0.113	0.075	0.048	0.019	0.011	0.004	0.002							4.00	4.53
111.0	21.0	2	0.045	0.129	0.177	0.184	0.159	0.120	0.079	0.043	0.020	0.011	0.005	0.002	0.001						4.08	4.70

Table III. Angular distribution results

Bombarding energy, E_b (lab) (MeV)	Target thickness W ($\mu g/cm^2$)	Cutter	Fractional cross section per unit angle $\Delta\sigma/\sigma\Delta\theta$ (deg^{-1}) — Ring number 1	2	3	4	5	6	7	8	9	10	11	12	13	14	15	16	17	18	$\langle\theta_L\rangle$	$\langle\theta_L^2\rangle^{1/2}$
			$Pr^{141}(C^{12}, 4n)Tb^{149g}$																				
>57.7[a]	27.2	2[b]	0.046	0.107	0.155	0.169	0.149	0.121	0.090	0.055	0.039	0.020	0.012	0.007	(0.004)[c]	(0.002)						4.51	5.15
>59.9[a]	30.3	1[b]	0.044	0.108	0.149	0.155	0.151	0.128	0.096	0.065	0.040	0.024	0.016	0.008	0.006	(0.004)						4.69	5.35
67.8	27.2	2[b]	0.033	0.089	0.132	0.149	0.150	0.133	0.100	0.074	0.045	0.030	0.018	0.012	0.008	0.005						4.97	5.64
70.1	30.3	2[b]	0.033	0.079	0.126	0.147	0.144	0.132	0.111	0.083	0.050	0.037	0.019	0.008	0.007	(0.005)						5.09	5.73
			$Nd^{146}(B^{10}, 7n)Tb^{149g}$																				
75.1	25.2	1[b]	(0.031)	0.067	0.092	0.112	0.122	0.118	0.111	0.089	0.083	0.064	0.042	0.026	← 0.016 →		← 0.002 →					5.97	6.77
102.4	25.2	2[b]	(0.024)	0.035	0.049	0.069	0.079	0.096	0.098	0.098	0.090	0.082	0.062	0.067	← 0.045 →		← 0.022 →		(0.011)			7.78	8.64
			$Nd^{146}(B^{11}, 8n)Tb^{149g}$																				
90.2	27.4	2[b]	(0.059)	0.078	0.095	0.114	0.126	0.122	0.101	0.088	0.062	0.056	0.034	0.019	0.012	0.008	(0.005)	(0.003)				5.54	6.37
103.7	27.4	2	(0.025)	0.047	0.073	0.099	0.104	0.112	0.109	0.112	0.074	0.075	0.051	0.037	0.028	0.013	0.010	(0.007)	(0.005)	(0.003)		6.69	7.53
103.7	89.0	1	(0.026)	0.046	0.069	0.090	0.099	0.108	0.101	0.096	0.081	0.071	0.057	0.043	0.037	0.023	0.017	(0.011)	(0.008)	(0.006)		7.13	8.07
103.7	0		0.025	0.048	0.074	0.100	0.107	0.113	0.111	0.110	0.078	0.075	0.048	0.034	0.024	0.008						6.50	7.29
112.8	27.4	1	(0.027)	0.043	0.067	0.083	0.101	0.113	0.108	0.094	0.085	0.075	0.053	0.044	0.036	0.025	0.023	(0.011)	(0.007)	(0.005)		7.13	8.04
			$Nd^{142}(C^{12}, 3n)Dy^{151}$																				
55.6	30.7	2[b]	0.048	0.130	0.159	0.173	0.160	0.115	0.084	0.046	0.031	0.014	0.010	0.006								4.23	4.83
70.1	30.7	1[b]	0.043	0.106	0.137	0.159	0.157	0.124	0.096	0.072	0.040	0.026	0.014	0.008	0.008							4.73	5.37
			$Nd^{142}(C^{12}, 4n)Dy^{150}$																				
70.1	30.7	1[b]	0.043	0.101	0.158	0.170	0.148	0.118	0.087	0.057	0.042	0.028	0.015	0.013	(0.009)							4.68	5.36
83.4	30.7	2[b]	0.033	0.092	0.134	0.153	0.151	0.130	0.099	0.070	0.047	0.030	0.017	0.011	0.006	0.004						4.92	5.57
92.0	30.7	1[b]	0.036	0.089	0.119	0.138	0.146	0.129	0.110	0.086	0.053	0.036	0.022	0.015	0.009	0.004						5.18	5.85
			$Nd^{142}(C^{12}, 5n)Dy^{149}$																				
83.4	30.7	2[b]	0.038	0.097	0.136	0.159	0.153	0.125	0.095	0.065	0.046	0.027	0.015	0.010	0.007	0.005						4.82	5.49
92.0	30.7	1[b]	0.038	0.093	0.132	0.152	0.146	0.132	0.102	0.075	0.049	0.030	0.021	0.011	0.007	0.004						4.98	5.64
100.6	30.7	1[b]	0.036	0.088	0.126	0.147	0.142	0.129	0.110	0.079	0.054	0.032	0.021	0.012	0.008	0.004						5.10	5.77
111.7	30.7	1[b]	← 0.053 →		0.110	0.132	0.137	0.130	0.110	0.088	0.064	0.043	0.028	0.018	0.010	← 0.005 →						5.43	6.15
122.8	30.7	1[b]	0.038	0.066	0.092	0.115	0.127	0.124	0.112	0.096	0.075	0.053	0.039	0.024	← 0.013 →		(0.004)					5.84	6.58

UCRL-10099 Rev.

Table III. Angular distribution results (Continued)

Bombarding energy, E_b (lab) (MeV)	Target thickness W ($\mu g/cm^2$)	Cutter	Fractional cross section per unit angle $\Delta\sigma/\sigma\Delta\theta$ (deg^{-1}) — Ring number →																		(θ_L)	$(\theta_L^2)^{1/2}$
			1	2	3	4	5	6	7	8	9	10	11	12	13	14	15	16	17	18		
										$Ce^{140}(O^{16}, 6n)Dy^{150}$													
101.0	36.4	1	0.063	0.134	0.166	0.183	0.167	0.120	0.079	0.024	0.032	0.008	0.008	0.004							4.03	4.59
111.0	21.0	2	0.045	0.129	0.177	0.184	0.159	0.120	0.079	0.043	0.020	0.011	0.005	0.002	0.001						4.08	4.70
121.1	36.4	2	0.047	0.114	0.151	0.177	0.166	0.131	0.080	0.054	0.040	0.021	0.013	0.006							4.44	5.06
130.4	36.4	2	0.038	0.110	0.158	0.177	0.153	0.124	0.089	0.059	0.036	0.022	0.007	0.003							4.42	4.97
139.2	21.0	2	0.040	0.108	0.164	0.171	0.160	0.120	0.094	0.055	0.033	0.019	0.008	0.003							4.37	4.92
										$Ce^{140}(O^{16}, 7n)Dy^{149}$													
111.0	21.0	2	0.043	0.120	0.161	0.172	0.158	0.120	0.086	0.055	0.030	0.016	0.007	0.005	0.002	0.0006					4.33	4.91
111.0	72.8	1	0.043	0.107	0.150	0.163	0.153	0.126	0.094	0.064	0.037	0.022	0.013	0.007	0.005	0.004					4.64	5.28
111.0	0		0.043	0.125	0.165	0.175	0.160	0.118	0.083	0.051	0.027	0.014	0.006	0.004	0.0004						4.20	4.76
121.1	36.4	1	0.045	0.122	0.154	0.170	0.158	0.128	0.092	0.058	0.034	0.013	0.010	0.006							4.39	4.96
130.4	36.4	1	0.047	0.114	0.157	0.169	0.156	0.125	0.093	0.058	0.035	0.020	0.008	0.007							4.43	5.01
139.2	36.4	1	0.046	0.110	0.153	0.166	0.153	0.135	0.091	0.059	0.037	0.019	0.009	0.007	0.003						4.50	5.09
139.2	21.0	2	0.043	0.113	0.157	0.171	0.156	0.127	0.088	0.061	0.033	0.018	0.008	0.004							4.38	4.95
163.0	36.4	1	0.039	0.091	0.130	0.149	0.146	0.135	0.110	0.077	0.053	0.030	0.017	0.009	0.003						4.93	5.55

[a] The energy-degrading foils were damaged by the beam.

[b] The second collimator was 1/8 in.

[c] Values in parentheses were obtained by graphical extrapolation.

Table IV. Average angles and energies

Bombarding energy (lab) E_b (MeV)	Corrected average angle $\langle\theta_L\rangle$ (deg.)	Corrected root mean square angle $\langle\theta_L^2\rangle$ (deg.)	Total available energy, $E_{cm}+Q$(MeV)	Average total neutron energy, T_n (MeV)	Average total photon energy, T_γ (MeV)
		$Pr^{141}(C^{12}, 4n)Tb^{149g}$			
> 57.7	3.94	4.49	> 6.2	< 6.2	> 0.0
> 59.9	4.08	4.64	> 7.9	< 6.8	> 1.1
67.8	4.40	4.98	15.2	9.0	6.2
70.1	4.48	5.02	17.3	9.4	7.9
		$Nd^{146}(B^{10}, 7n)Tb^{149g}$			
75.1	5.54	6.25	15.7	12.8	2.9
102.4	7.35	8.12	41.2	29.5	11.7
		$Nd^{146}(B^{11}, 8n)Tb^{149g}$			
90.2	5.10	5.83	17.8	14.6	3.2
103.7	6.50	7.29	30.3	26.3	4.0
112.8	6.94	7.80	38.8	32.8	6.0
		$Nd^{142}(C^{12}, 3n)Dy^{151}$			
55.6	3.61	4.11	9.3	5.0	4.3
70.1	4.11	4.66	22.6	8.2	14.4
		$Nd^{142}(C^{12}, 4n)Dy^{150}$			
70.1	4.06	4.65	14.7	8.1	6.6
83.4	4.30	4.86	27.0	10.5	16.5
92.0	4.56	5.14	34.9	13.0	21.9

Table IV. Average angles and energies (Cont.)

Bombarding energy (lab) E_b (MeV)	Corrected average angle $\langle\theta_L\rangle$ (deg.)	Corrected root mean square angle $\langle\theta_L^2\rangle$ (deg.)	Total available energy, $E_{cm}+Q$ (MeV)	Average total neutron energy, T_n (MeV)	Average total photon energy, T_γ (MeV)
		$Nd^{142}(C^{12}, 5n)Dy^{149}$			
83.4	4.20	4.78	16.8	10.1	6.7
92.0	4.36	4.93	24.7	11.9	12.8
100.6	4.48	5.06	32.7	13.7	19.0
111.7	4.81	5.44	42.9	17.5	25.4
122.8	5.22	5.87	53.1	22.5	30.6
		$Nd^{144}(C^{12}, 5n)Dy^{151}$			
77.5	4.48	5.23	15.2	11.1	4.1
83.4	4.57	5.25	20.7	12.2	8.5
94.0	4.88	5.47	30.5	14.9	15.6
		$Nd^{144}(C^{12}, 6n)Dy^{150}$			
94.0	4.87	5.64	22.6	15.8	6.8
99.7	4.85	5.52	27.8	16.0	11.8
111.6	5.19	5.92	38.8	20.6	18.2
122.8	5.32	6.06	49.2	23.8	25.4
		$Nd^{144}(C^{12}, 7n)Dy^{149}$			
94.0	4.66	5.35	12.4	14.1	-1.7
99.7	4.68	5.39	17.6	15.2	2.4
111.6	5.03	5.74	28.6	19.3	9.3
122.8	5.09	5.84	39.0	21.9	17.1

Table IV. Average angles and energies (Cont.)

Bombarding energy (lab) E_b (MeV)	Corrected average angle $\langle\theta_L\rangle$ (deg.)	Corrected root mean square angle $\langle\theta_L^2\rangle$ (deg.)	Total available energy, $E_{cm}+Q$(MeV)	Average total neutron energy, T_n (MeV)	Average total photon energy, T_γ (MeV)
		$Ce^{140}(O^{16}, 5n)Dy^{151}$			
89.7	3.63	4.16	15.4	11.0	4.4
101.0	3.78	4.27	25.5	13.0	12.5
111.0	3.95	4.55	34.5	16.1	18.4
		$Ce^{140}(O^{16}, 6n)Dy^{150}$			
101.0	3.81	4.33	17.6	13.3	4.3
111.0	3.95	4.55	26.6	16.1	10.5
121.1	4.22	4.80	35.7	19.6	16.1
130.4	4.20	4.71	44.0	20.3	23.7
139.2	4.24	4.77	51.9	22.3	29.6
		$Ce^{140}(O^{16}, 7n)Dy^{149}$			
111.0	4.20	4.76	16.4	17.8	-1.4
121.1	4.17	4.70	25.5	19.0	6.5
130.4	4.21	4.75	33.8	20.9	12.9
139.2	4.26	4.82	41.7	23.0	18.7
163.0	4.71	5.29	63.1	32.3	30.8

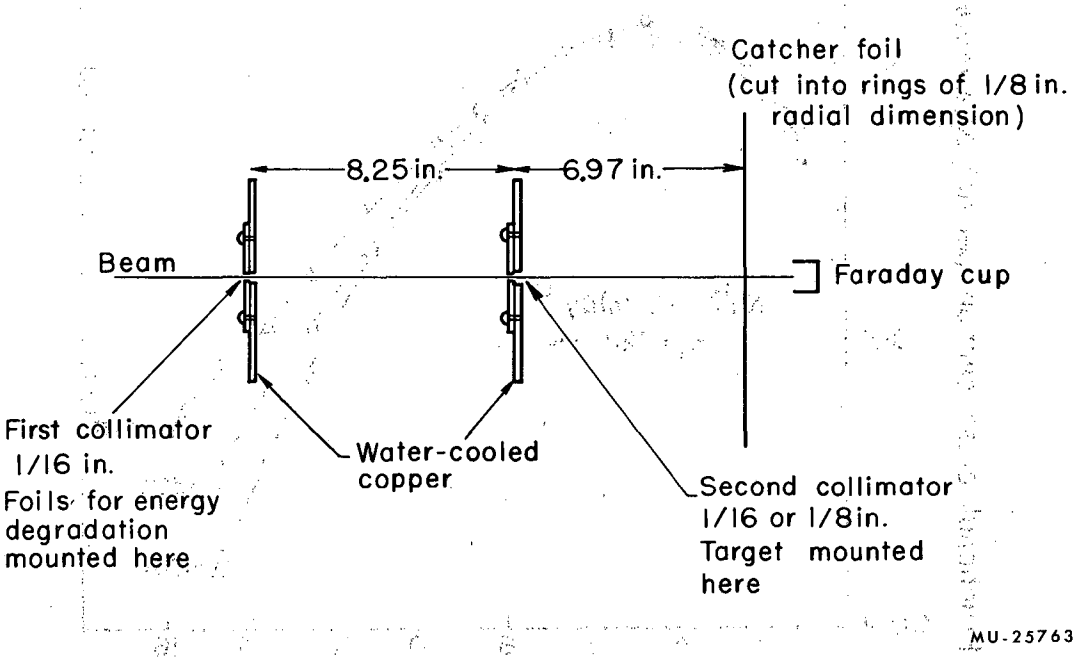

Fig. 1. Schematic diagram of the apparatus used for angular-distribution measurements.

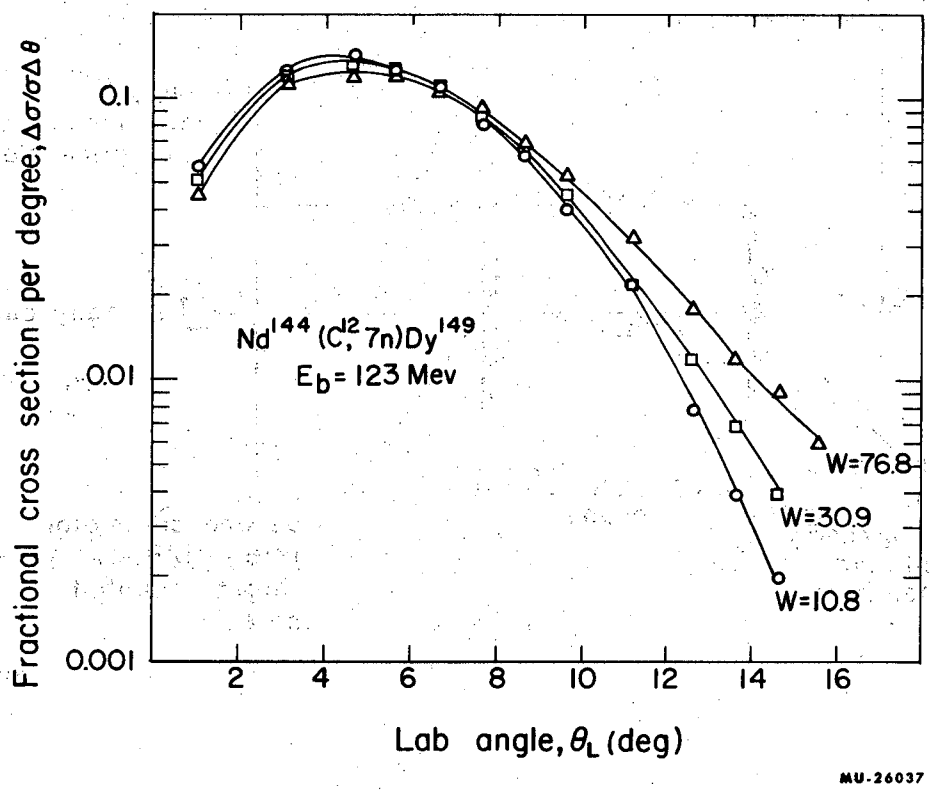

Fig. 2. The effect of target thickness on observed angular-distribution. The target thickness W is denoted for each curve in $\mu g/cm^2$. These data are for the reaction Nd^{144} + 123-MeV $C^{12} \rightarrow Dy^{149}$ + 7n.

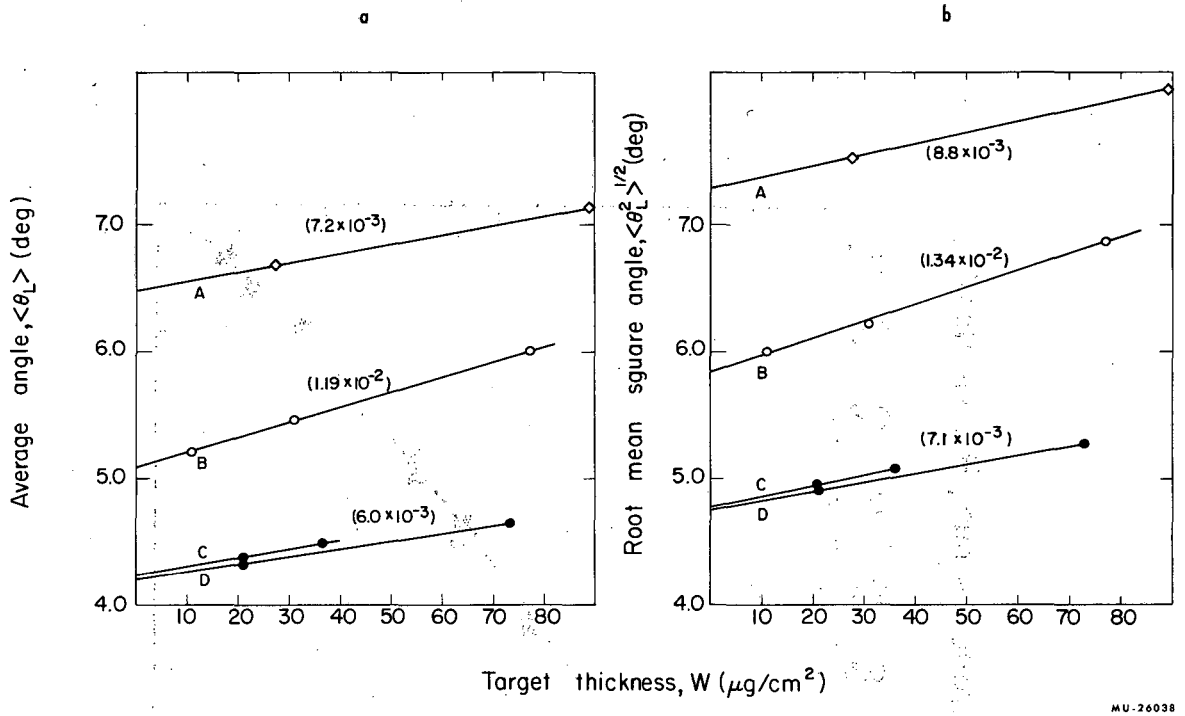

Fig. 3. The dependence of (a) the average angle $\langle\theta_L\rangle$ and (b) the root-mean-square angle $\langle\theta_L^2\rangle^{1/2}$ on target thickness W. Curves A are for the reaction Nd^{146} + 104-MeV $B^{11} \rightarrow Tb^{149g}$ + 8n;
B for Nd^{144} + 123-MeV $C^{12} \rightarrow Dy^{149}$ + 7n;
C for Ce^{140} + 139-MeV $O^{16} \rightarrow Dy^{149}$ + 7n; and
D for Ce^{140} + 111-MeV $O^{16} \rightarrow Dy^{149}$ + 7n.
The numbers in parentheses denote the slopes of the curves in deg/(μg/cm^2).

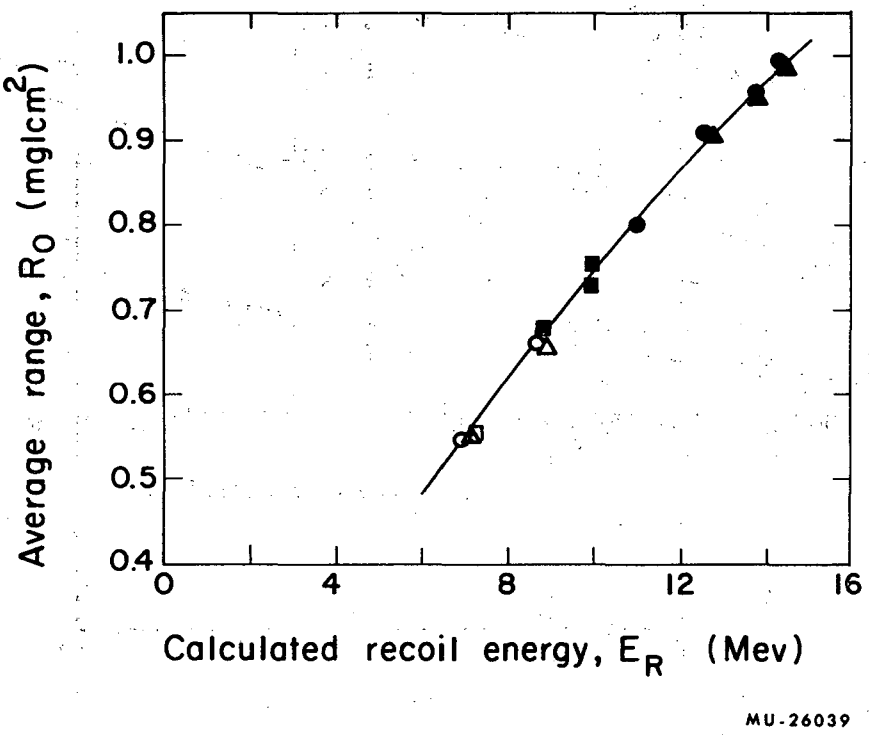

Fig. 4. Average range R_0 in Al vs the calculated recoil energy E_R. Symbols are as follows: Dy^{151} ⊡ ; Dy^{150} △ ; Dy^{149} ⊙ . Open symbols are for the reactions C^{12} + Nd^{144}; closed, for O^{16} + Ce^{140}. The smooth curve is from reference 3.

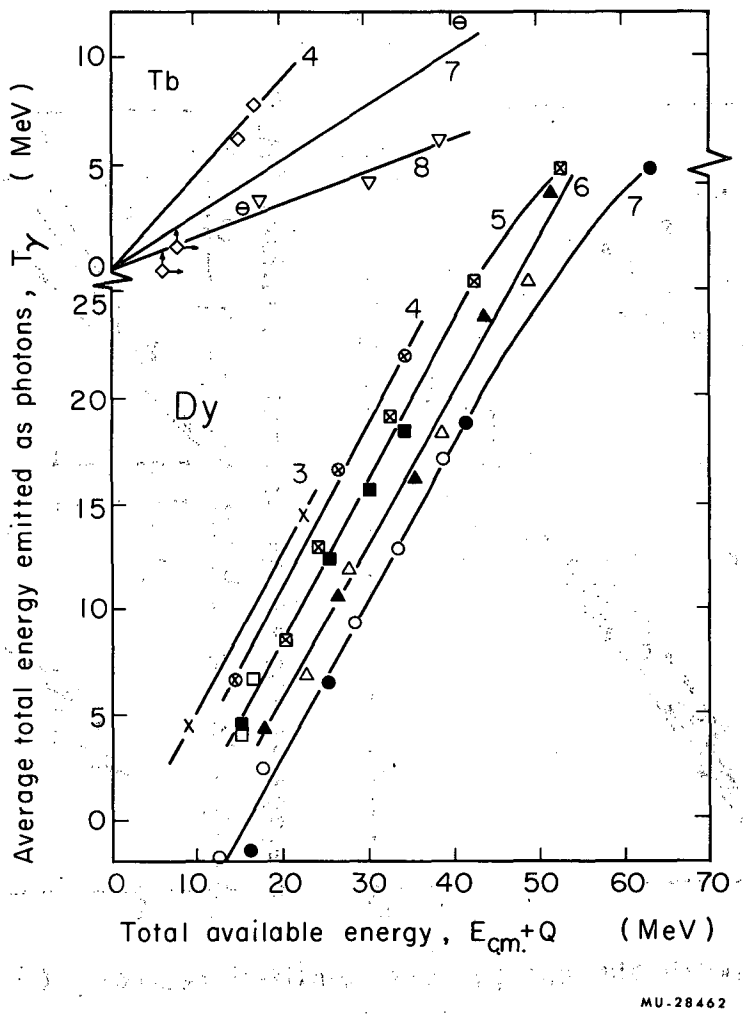

Fig. 5. Total photon energy vs total available energy. The upper curves are for Tb compound nuclei and the product Tb^{149g}. The lower curves are for Dy compound nuclei and products Dy^{149}, Dy^{150}, and Dy^{151}. The number of emitted neutrons is indicated for each curve. Symbols are as follows:
$Pr^{141}(C^{12}, 4n)Tb^{149g}$ ◇ ; $Nd^{146}(B^{10}, 7n)Tb^{149g}$ θ;
$Nd^{146}(B^{11}, 8n)Tb^{149g}$ ▽ ; $Nd^{142}(C^{12}, 3n)Dy^{151}$ X ;
$Nd^{142}(C^{12}, 4n)Dy^{150}$ ⊗ ; $Nd^{142}(C^{12}, 5n)Dy^{149}$ ⊠ ;
$Nd^{144}(C^{12}, 5n)Dy^{151}$ □ ; $Nd^{144}(C^{12}, 6n)Dy^{150}$ △ ;
$Nd^{144}(C^{12}, 7n)Dy^{149}$ ○ ; $Ce^{140}(O^{16}, 5n)Dy^{151}$ ■ ;
$Ce^{140}(O^{16}, 6n)Dy^{150}$ ▲ ; $Ce^{140}(O^{16}, 7n)Dy^{149}$ ▲ .

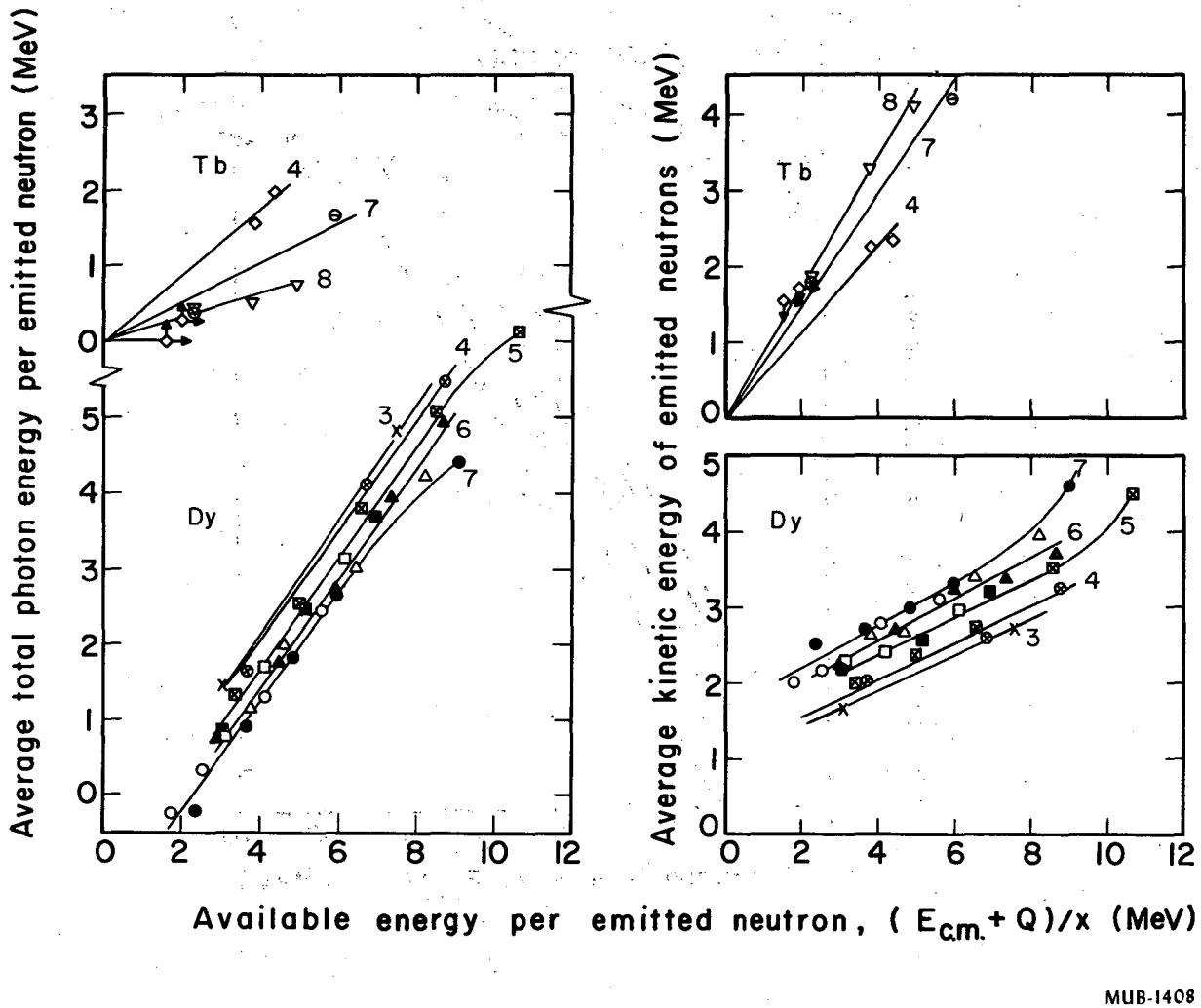

Fig. 6. Average total energy of photons (a) and average energy of neutrons (b) vs available energy per emitted neutron $(E_{c.m.} + Q)/x$ for reactions in which x neutrons are emitted. Symbols are as in Fig. 5.